



What Caused Recent Shifts in Tropical Pacific Decadal Sea-Level Trends?

Christopher G. Piecuch¹ , Philip R. Thompson² , Rui M. Ponte³ , Mark A. Merrifield⁴ , and Benjamin D. Hamlington⁵

¹Physical Oceanography Department, Woods Hole Oceanographic Institution, Woods Hole, MA, USA, Department of Oceanography, ²University of Hawai'i at Mānoa, Honolulu, HI, USA, ³Atmospheric and Environmental Research, Inc., Lexington, MA, USA, ⁴Scripps Institution of Oceanography, La Jolla, CA, USA, ⁵Jet Propulsion Laboratory, Pasadena, CA, USA

Key Points:

- Sea level in the western tropical North Pacific and eastern and central equatorial Pacific underwent decadal variation over 1993–2015
- This decadal variation reflects ocean heat storage related to ocean heat transport and local surface heat flux due to anomalous wind stress
- Contributions from air-sea heat exchange arise from latent heat flux associated with wind-stress-related sea-surface temperature changes

Supporting Information:

- Supporting Information S1

Correspondence to:

C. G. Piecuch,
cpiecuch@whoi.edu

Citation:

Piecuch, C. G., Thompson, P. R., Ponte, R. M., Merrifield, M. A., & Hamlington, B. D. (2019). What caused recent shifts in tropical Pacific decadal sea-level trends?. *Journal of Geophysical Research: Oceans*, 124, 7575–7590. <https://doi.org/10.1029/2019JC015339>

Received 31 MAY 2019

Accepted 8 OCT 2019

Accepted article online 16 OCT 2019

Published online 11 NOV 2019

Abstract Satellite altimetry reveals substantial decadal variability in sea level ζ across the tropical Pacific during 1993–2015. An ocean state estimate that faithfully reproduces the observations is used to elucidate the origin of these low-frequency tropical Pacific ζ variations. Analysis of the hydrostatic equation reveals that recent decadal ζ changes in the tropical Pacific are mainly thermosteric in nature, related to changes in upper-ocean heat content. A forcing experiment performed with the numerical model suggests that anomalous wind stress was an important driver of the relevant heat storage and thermosteric variation. Closed budget diagnostics further clarify that the wind-stress-related thermosteric ζ variation resulted from the joint actions of large-scale ocean advection and local surface heat flux, such that advection controlled the budget over shorter, intraseasonal to interannual time scales, and local surface heat flux became increasingly influential at longer decadal periods. In particular, local surface heat flux was important in contributing to a recent reversal of decadal ζ trends in the tropical Pacific. Contributions from local surface heat flux partly reflect damping latent heat flux tied to wind-stress-driven sea-surface-temperature variations.

1. Introduction

Sea level ζ is an informative measure of ocean circulation and climate, related to surface geostrophic flows, and subsurface heat, salt, and mass storage. Previous studies sought to identify the causes of regional ζ changes during the last quarter century observed by satellite altimetry (e.g., Cazenave et al., 2018). Changes in ζ across the tropical Pacific Ocean received particular attention. Trends in ζ over the western tropical Pacific since 1993 were higher than the global-mean ζ trend, with the opposite being true along the eastern tropical Pacific (Cazenave & Llovel, 2010; Hamlington et al., 2016; Meyssignac et al., 2012; Palanisamy et al., 2015; Stammer et al., 2013). This spatial structure was interpreted largely in terms of adiabatic internal redistribution and anomalous heat transport driven by the overlying equatorial wind field and wind stress curl off the equator, such that the higher ζ trends observed in the western tropical Pacific were due to regional accumulation of heat in the upper ocean (McGregor et al., 2012; Merrifield, 2011; Merrifield & Maltrud, 2011; Merrifield et al., 2012; Moon & Song, 2013; Moon et al., 2013; Qiu & Chen, 2012; Timmermann et al., 2010).

This understanding of tropical Pacific ζ changes is interesting given interpretations of the recent surface warming slowdown. Between the late 1990s and early 2010s, globally averaged surface temperature plateaued or decreased slightly (Fyfe et al., 2016; Karl et al., 2015; Medhaug et al., 2017; Xie & Kosaka, 2017). Coupling between the trade winds and eastern tropical Pacific sea-surface temperatures—manifested in a stronger Walker circulation, a cooler eastern tropical Pacific sea surface, and more intense subduction and upwelling processes related to the subtropical overturning circulation cell (cf. Cheng et al., 2007; Feng et al., 2010; McPhaden & Zhang, 2002)—were identified as crucial to the slowdown (Delworth et al., 2015; England et al., 2014; Kosaka & Xie, 2013; McGregor, 2014; Meehl et al., 2013; Watanabe et al., 2014). Because sea-water expands when it warms and contracts when it cools, the sea-surface heat exchanges required by such coupled air-sea interactions imply ζ changes across the tropical Pacific. However, excepting a few papers that are treated below in the context of our results (e.g., Fukumori & Wang, 2013; Moon & Song, 2013), past

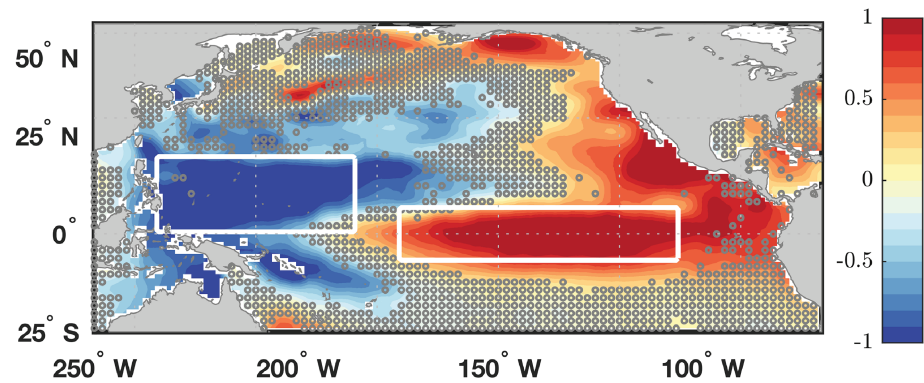


Figure 1. Map of acceleration (positive) or deceleration (negative) in ζ from monthly satellite altimeter data 1993–2015 (mm/year). Values are computed as twice the quadratic coefficient from a simultaneous least squares fit of a second-order polynomial plus seasonal cycle (annual and semiannual harmonics) to the altimetry data. The white outlined boxes are the WTNP (left) and ECEP (right) study regions. Gray dots indicate where values are not statistically significant at the $p = 0.10$ level.

altimeter studies did not consider whether such diabatic processes were relevant to tropical Pacific ζ variability (McGregor et al., 2012; Merrifield, 2011; Merrifield & Maltrud, 2011; Merrifield et al., 2012; Qiu & Chen, 2012; Timmermann et al., 2010).

Hamlington et al. (2016) hypothesized that a shift in Pacific ζ is ongoing, such that the dominant spatial pattern of ζ trends typifying the earlier part of the altimeter period has reversed, with ζ rising in the eastern and central equatorial Pacific and falling in the western tropical Pacific during recent years. This trend reversal is visualized by mapping ζ accelerations and decelerations over 1993–2015, which are computed as twice the quadratic coefficient of a simultaneous least squares fit of a second-order polynomial and seasonal cycle to the altimetry data over the Pacific Ocean (Figure 1). Enhanced ζ decelerations (approximately -1 mm/year²) appear broadly across the western tropical North Pacific, consistent with the ζ rise during the earlier part of the record followed by ζ fall later on, while elevated ζ accelerations (~ 1 mm/year²) emerge along the eastern and central equatorial Pacific, consistent with the initial ζ fall followed by subsequent ζ rise. Although they suggested that such ζ behavior could persist into the future, leading to ζ increase over the eastern and central equatorial Pacific and ζ decrease over the western tropical North Pacific in the years to come, Hamlington et al. (2016) did not inquire into the physical processes underlying the recent tropical Pacific decadal ζ variability, which remain to be established.

The Hamlington et al. (2016) analysis represents a timely occasion to revisit the causes of recent decadal ζ variability in the tropical Pacific. Do recent decadal ζ variations over the tropical Pacific mainly reflect wind forcing and internal redistribution by ocean transports, as suggested in past altimeter ζ studies, or are air-sea heat fluxes also relevant, as implied by current understanding of the surface warming slowdown? If surface heat fluxes are relevant, what is their nature? To address these questions, we use a recent global ocean state estimate from the ECCO (Estimating the Circulation and Climate of the Ocean) consortium (Forget et al., 2015), which represents a coherent synthesis of a general circulation model with most available ocean data. Exploiting the numerical machinery and physical consistency afforded by the model, we perform a set of forcing experiments and diagnose budgets to paint a detailed, rich, and quantitative portrait of the physics underpinning recent tropical Pacific decadal ζ changes. Note that we do not attempt to determine whether long-term shifts in ζ trends are ongoing and will persist into the future; rather, we seek to identify the mechanisms of the ζ changes highlighted by Hamlington et al. (2016) during the 1993–2015 period. The remainder of this paper is structured as follows: In section 2, we describe the estimate and compare to data; in section 3, we present results of the forcing experiments and budget calculations; and in section 4, we discuss and interpret our results and point to future work.

2. Methods

2.1. Ocean State Estimate

ECCO Version 4 (ECCOv4) is the latest nonlinear inverse modeling framework for global ocean state estimation from the ECCO consortium (Forget et al., 2015). State estimates are produced using the method of

Lagrange multipliers; a hydrostatic, Boussinesq general circulation model (Marshall et al., 1997) is fit to myriad in situ and remotely sensed observations (altimetry, Argo, etc.) by iteratively adjusting a control vector comprising initial conditions, boundary conditions, and mixing coefficients. The horizontal model grid has 1° nominal resolution over the global ocean, reducing to $\sim 0.3^\circ$ in latitude near the equator. Fifty vertical layers are used, with thickness ranging from 10 m near the surface to ~ 450 m in the abyss. Bulk formulae are used for the surface heat and freshwater forcing (Large & Yeager, 2004), whereas wind stress is prescribed directly for the surface momentum forcing. Atmospheric variables (temperature, humidity, precipitation, radiation, etc.) used in the forcing are first taken from an atmospheric reanalysis (Dee et al., 2011) and subsequently adjusted as part of the estimation. Large-scale effects of unresolved small-scale processes are parameterized (Gaspar et al., 1990; Gent & McWilliams, 1990; Redi, 1982). The estimate, while constrained to data, is a freely running model solution; it maintains physical consistency and obeys conservation laws, with no artificial sources or sinks, facilitating meaningful budget analyses (e.g., Piecuch, 2017).

We use the recent ECCOv4 Release 3 solution covering 1992–2015 (Fukumori et al., 2017). Relative to the earlier Release 1 estimate spanning 1992–2011 (Forget et al., 2015), Release 3 incorporates additional data constraints (e.g., Aquarius, Gravity Recovery and Climate Experiment) and control parameters (horizontal velocity and ζ initial conditions), uses a modified cost function (separating time-independent and time-dependent components, reducing spatial correlation, and accounting for variable grid spacing), and includes a geothermal flux bottom boundary condition (Piecuch et al., 2015). See Fukumori et al. (2017, 2018) for more details. Given the weaker data constraints during 1992 (e.g., TOPEX/Poseidon did not fly until late that year), we consider monthly ECCOv4 Release 3 output for 1993–2015.

2.2. Processing, Statistics, and Significance

We are interested in low-frequency variability, particularly the decadal ζ trend reversal discussed by Hamlington et al. (2016). To quantify the shift in decadal trends, we simultaneously fit second-order polynomials and mean seasonal cycles (annual and semiannual harmonics) to the time series using least squares. We take twice the quadratic coefficient of the fit—which we call the “acceleration” or “deceleration” depending on whether the sign is positive or negative—as a measure of the trend reversal. This construct is a statistical summary of decadal variation during 1993–2015 and should not be taken as indicative of future behavior. To account for the effects of correlated noise (e.g., Bos et al., 2014), we estimate the significance (p values) of coefficients through repeated simulations with synthetic time series and Fourier phase scrambling, as described in Piecuch et al. (2017). Coefficients with p values < 0.10 based on a one-sided test are regarded as statistically significant. Note that, given the length of the time series, long-term secular change cannot be distinguished from stationary multidecadal variability. To isolate spacetime anomalies, we remove time series of spatial-mean values over the global ocean as well as local time-mean values from time series at every location.

2.3. Comparison to Observations

To assess the realism of the state estimate, we compare to altimetry data. We use $1^\circ \times 1^\circ$ monthly gridded ζ fields spanning 1993–2015 from the Commonwealth Scientific and Industrial Research Organisation (CSIRO), which are derived from the reference altimeter missions (TOPEX/Poseidon, Jason altimeters). The grids are corrected for air-pressure effects and glacial isostatic adjustment (Church & White, 2011). Our comparisons, as well as all subsequent analysis, target two regions showing strong decadal ζ variability: the western tropical North Pacific (WTNP; 125° – 175° E, 0° – 20° N) and the eastern and central equatorial Pacific (ECEP; 105° – 175° W, 7.5° S to 7.5° N). See the white boxes in Figure 1. Similar regions were highlighted in Hamlington et al. (2016).

Figure 2 shows ζ time series averaged over the WTNP and ECEP from ECCOv4 and CSIRO. Regional ζ fluctuations occur over a range of time scales, such that subtler decadal and longer changes superimpose on more pronounced seasonal and interannual variations. The corresponding model and data ζ curves are strikingly similar, and the model explains 94–98% of the monthly data variance, depending on region, revealing that the state estimate is an excellent fit to the altimeter data. In particular, ECCOv4 and CSIRO show clear agreement in terms of ζ behavior at low frequencies. Over the WTNP, CSIRO and ECCOv4 ζ time series, respectively, show significant decelerations of -1.04 and -1.25 mm/year² (Table 1), reflecting the change from positive to negative ζ trends during the course of the altimeter period. In contrast, data and model ζ curves, respectively, exhibit significant accelerations of 0.86 and 0.80 mm/year² (Table 1) over the ECEP,

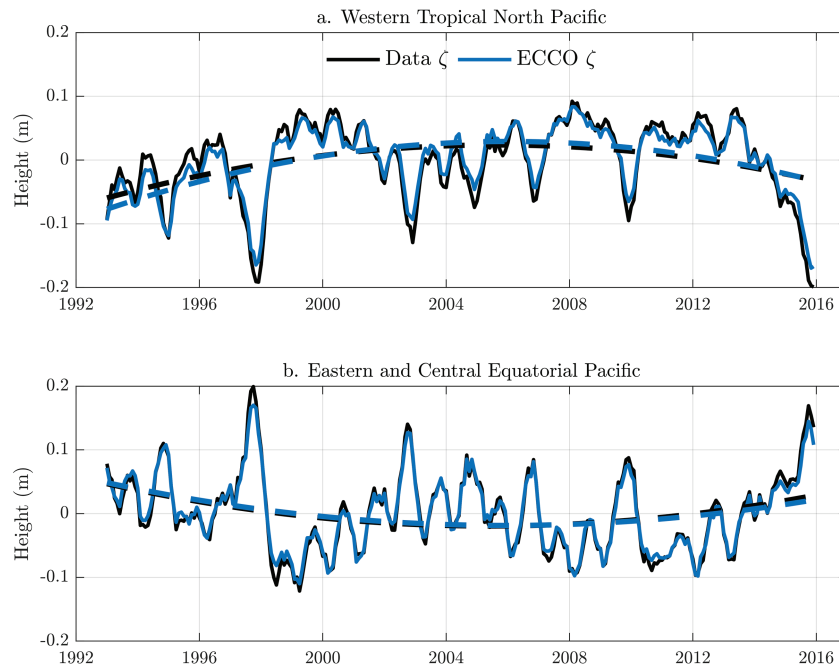


Figure 2. Monthly ζ time series from satellite altimetry (CSIRO; black) and the state estimate (ECCOv4; blue) averaged over the (a) WTNP and (b) ECEP. Dashed curves are quadratic components from a simultaneous fit of a second-order polynomial plus seasonal cycle to the series.

indicating the shift from negative to positive rates of ζ change over time. These results are consistent with the broad acceleration and deceleration patterns in Figure 1.

Table 1
Accelerations (Positive) and Decelerations (Negative) in ζ During 1993–2015 Over the Study Regions

Term	WTNP	ECEP
ζ (CSIRO)	−1.04 (0.07)	0.86 (0.06)
ζ (ECCOv4)	−1.25 (0.08)	0.80 (0.08)
ζ_T	−1.22 (0.08)	0.75 (0.12)
ζ_S	−0.09 (0.26)	0.02 (0.46)
ζ_M	0.06 (0.06)	0.05 (0.01)
ζ_N	−0.02 (0.03)	0.01 (0.17)
$\zeta_T^{\tau'}$	−1.15 (0.10)	0.70 (0.07)
$\zeta_T^{\bar{\tau}'}$	−0.07 (0.22)	0.05 (0.42)
$\mathcal{A}^{\tau'}$	−0.16 (0.20)	−0.51 (0.43)
$\mathcal{M}^{\tau'}$	0.11 (0.27)	−0.05 (0.42)
$\mathcal{F}^{\tau'}$	−1.10 (0.11)	1.27 (0.32)
$\mathcal{F}_E^{\tau'}$	−0.84 (0.10)	0.96 (0.32)
$\mathcal{F}_H^{\tau'}$	−0.21 (0.11)	0.22 (0.38)
$\mathcal{F}_S^{\tau'}$	0.12 (0.02)	−0.10 (0.39)
$\mathcal{F}_L^{\tau'}$	−0.15 (0.11)	0.16 (0.36)
$\mathcal{F}_P^{\tau'}$	−0.03 (0.16)	0.03 (0.36)

Note. Numbers outside parentheses are the accelerations or decelerations with units of mm/year². Numbers within parentheses are the corresponding p values.

The ECCOv4 solution also compares favorably to surface currents from Ocean Surface Current Analyses Real-time (OSCAR; Bonjean & Lagerloef, 2002), subsurface temperatures and currents from the Tropical Atmosphere Ocean/Triangle Trans-Ocean Buoy Network (TAO/TRITON; Ando & Kuroda, 2002; McPhaden et al., 1998), and surface heat fluxes from Objectively Analyzed air-sea Fluxes (OAFflux; Yu & Weller, 2007) over the study region (see Text S1 and Figures S1–S17 in the supporting information). Such comparisons are not independent. Altimetry is used in the state estimation. Both ECCOv4 and OSCAR are based on common data sets. While they are not used to constrain ECCOv4, temperatures and currents from TAO/TRITON are coupled to other ocean variables, observations of which are included in the state estimation (e.g., satellite sea-surface height, and temperature). Nevertheless, these comparisons bespeak the realism of the solution—ECCOv4 is a spatiotemporally complete, physically consistent embodiment of the oceanic variability observed over the WTNP and ECEP during the study period. We focus on the ECCOv4 solution for the remainder of the paper, giving a detailed diagnosis of the processes at work in the estimate, in order to shed light on the causal mechanisms responsible for the observed behavior.

3. Results

3.1. Hydrostatic Decomposition of ζ

To identify the processes giving rise to the ζ changes (Figure 2), an informative approach is to decompose ζ into contributions from heat, salt, and mass storage using the hydrostatic equation (Gill & Niiler, 1973). For an ocean with a nonlinear free surface and a rescaled height coordinate, as in ECCOv4, ζ changes are partitioned as (see Appendix A)

$$\zeta = \zeta_M + \zeta_T + \zeta_S + \zeta_N. \quad (1)$$

Table 2
Definitions of Symbols Used in the Paper

Symbol	Description (relevant equation)
ζ	Sea level
ζ_T	Thermosteric height contribution to ζ changes (equation (1))
ζ_S	Halosteric height contribution to ζ changes (equation (1))
ζ_M	Ocean mass contribution to ζ changes (equation (1))
ζ_N	Nonlinear correction to hydrostatic ζ decomposition (equation (1))
$\zeta_T^{\tau'}$	ζ_T changes occurring under anomalous wind-stress forcing (equation (2))
$\zeta_T^{\bar{\tau}}$	ζ_T changes occurring under climatological wind-stress forcing (equation (2))
$\mathcal{A}^{\tau'}$	Large-scale ocean advection contribution to $\zeta_T^{\tau'}$ changes (equation (3))
$\mathcal{M}^{\tau'}$	Parameterized small-scale mixing contribution to $\zeta_T^{\tau'}$ changes (equation (3))
$\mathcal{F}^{\tau'}$	Total surface heat flux contribution to $\zeta_T^{\tau'}$ changes (equation (3))
$\mathcal{F}_E^{\tau'}$	Latent heat flux contribution to $\zeta_T^{\tau'}$ changes (equation (4))
$\mathcal{F}_H^{\tau'}$	Sensible heat flux contribution to $\zeta_T^{\tau'}$ changes (equation (4))
$\mathcal{F}_S^{\tau'}$	Shortwave heat flux contribution to $\zeta_T^{\tau'}$ changes (equation (4))
$\mathcal{F}_L^{\tau'}$	Longwave heat flux contribution to $\zeta_T^{\tau'}$ changes (equation (4))
$\mathcal{F}_P^{\tau'}$	Precipitation heat flux contribution to $\zeta_T^{\tau'}$ changes (equation (4))
θ	Potential temperature
θ_0	Sea-surface temperature
σ	Standard deviation

Here ζ_M , ζ_T , and ζ_S are ζ changes related to mass, heat, and salt storage, respectively, and ζ_N is a correction term that appears on account of the nonlinear seawater equation of state and free-surface boundary condition (see Appendix A). Note that all symbols used in the text are defined in Table 2 for reference.

Figure 3 shows hydrostatic ζ components averaged spatially across the WTNP and ECEP. Time series of ζ and ζ_T are nearly identical, and the former explains 93–96% of the latter's total monthly variance, depending on region. Further, ζ_T accounts for 97% of the ζ deceleration in the WTNP, and 94% of the ζ acceleration in the ECEP (Table 1). This reveals that the ζ changes are thermosteric in nature and related to heat storage. In comparison, ζ_M , ζ_S , and ζ_N show more muted variability (standard deviations $\sigma < 1$ cm) relative to ζ and ζ_T ($\sigma \sim 5$ cm), and much weaker accelerations and decelerations (Table 1), meaning that these other effects on ζ are negligible. These results are consistent with previous studies finding that low-frequency ζ changes in these regions are reflective of ocean heat storage (e.g., Moon & Song, 2013; Peyser & Yin, 2017; Timmermann et al., 2010).

To isolate the regions of relevant low-frequency ocean temperature changes, Figure 4 shows accelerations and decelerations during 1993–2015 in potential temperature θ averaged zonally across the WTNP and ECEP versus latitude and depth. A broad area of θ deceleration is apparent in the WTNP (Figure 4a), with the most pronounced (but generally not significant) values (approximately $-0.02^\circ\text{C}/\text{year}^2$) concentrated below the surface, from 100-m to 300-m depth, between the mean 14 and 28°C isotherms. A distinct structure of decadal θ variation characterizes the ECEP (Figure 4b), with strong θ accelerations ($\sim 0.02^\circ\text{C}/\text{year}^2$) found near the surface, within the upper 150 m or so, mainly above the 20°C mean isotherm. England et al. (2014) highlighted opposing θ trends over roughly these same ocean regions and depth ranges as being relevant to the recent surface warming slowdown (cf. their Figures 3 and S6).

3.2. Forcing Mechanisms of ζ_T

To determine what drives the ζ_T changes (Figure 3), we perform an additional model experiment. Recall that whereas surface heat and freshwater fluxes in ECCOv4 are determined by bulk formulae, surface momentum flux is prescribed by specifying wind stress directly (Forget et al., 2015). We run a model perturbation experiment setting surface wind stress to climatology (a mean year of six-hourly values during 1992–2015), but allowing other surface atmospheric state variables (temperature, humidity, precipitation, radiation, etc.) to vary. Aside from the modified wind stress, no other changes are made to the model setup relative to ECCOv4. Forget and Ponte (2015) performed a similar perturbation experiment based on an earlier ECCOv4

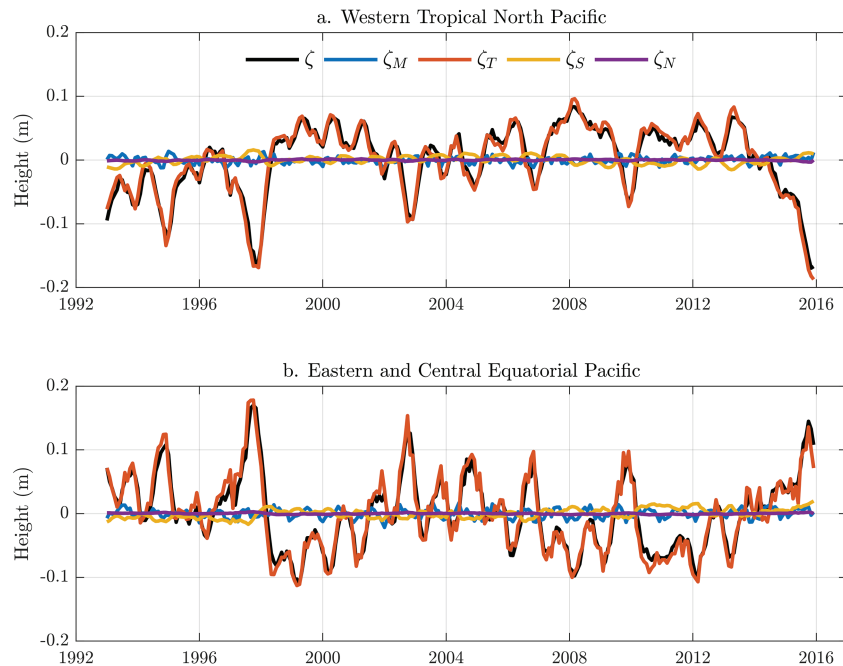


Figure 3. Decomposition of ζ (black) into contributions from ocean mass ζ_M (blue), thermosteric height ζ_T (orange), halosteric height ζ_S (yellow), and a nonlinear correction term ζ_N (purple) averaged over the (a) WTNP and (b) ECEP from ECCOv4. See equation (1) for breakdown.

iteration. In an attempt to quantify the role of forcing by wind stress, we take the difference between output from ECCOv4 and the perturbation run,

$$\zeta_T^{r'} \doteq \zeta_T - \zeta_T^{\bar{r}}, \quad (2)$$

where $\zeta_T^{\bar{r}}$ represents ζ_T changes from the perturbation experiment, produced under climatological wind stress. We interpret $\zeta_T^{r'}$ as reflecting ζ_T changes due to anomalous wind stress. Note that this interpretation implicitly assumes a linear ocean response in the sense that the influence of wind-stress forcing can be separated from the effects of the other surface atmospheric state variables. In what follows, we proceed under this assumption of linearity and separability, regarding differences between ECCOv4 and the perturbation run as due to wind stress, but we return to the topic of possible nonlinear effects later on in the discussion.

Time series of WTNP and ECEP ζ_T , $\zeta_T^{r'}$, and $\zeta_T^{\bar{r}}$ (Figure 5) make clear that the mechanisms responsible for driving ζ_T changes depend on time scale. Regional $\zeta_T^{\bar{r}}$ time series show clear annual and semiannual sinusoids, which largely explain the seasonal cycles in the WTNP and ECEP ζ_T curves. However, $\zeta_T^{\bar{r}}$ cannot explain the dominant nonseasonal ζ_T behavior of interest. Rather, most of the overall large-scale monthly ζ_T variance (88% in the WTNP and 79% in the ECEP) is attributable to $\zeta_T^{r'}$ changes related to anomalous wind-stress forcing. Particularly noteworthy, $\zeta_T^{r'}$ accounts for 94% of the ζ_T deceleration in the WTNP, and 93% of the ζ_T acceleration in the ECEP during 1993–2015, whereas regional $\zeta_T^{\bar{r}}$ accelerations and decelerations during that period are an order of magnitude smaller, and not statistically significant (Table 1). These results suggest that wind stress is the dominant driver of nonseasonal WTNP and ECEP ζ_T changes and that other surface atmospheric forcing variables are negligible. These results are consistent with previous studies arguing that recent tropical Pacific ζ changes are related to shifts in the prevailing trade winds (McGregor et al., 2012; Merrifield, 2011; Merrifield & Maltrud, 2011; Timmermann et al., 2010).

3.3. Budget Analysis of $\zeta_T^{r'}$

Large-scale, low-frequency ζ variability over the WTNP and ECEP is related to upper-ocean heat storage and anomalous wind-stress forcing (Figures 3 and 5). However, given the model formulation, it does not necessarily follow that this ζ variability is wholly attributable to adiabatic redistribution of heat content by ocean circulation. The bulk formulae used in the model to determine sensible, latent, and longwave heat fluxes are functions not only of the surface atmospheric state (e.g., air temperature, specific humidity, and wind speed) but also of sea-surface temperature θ_0 (Large & Yeager, 2004). Note that the wind speeds used in

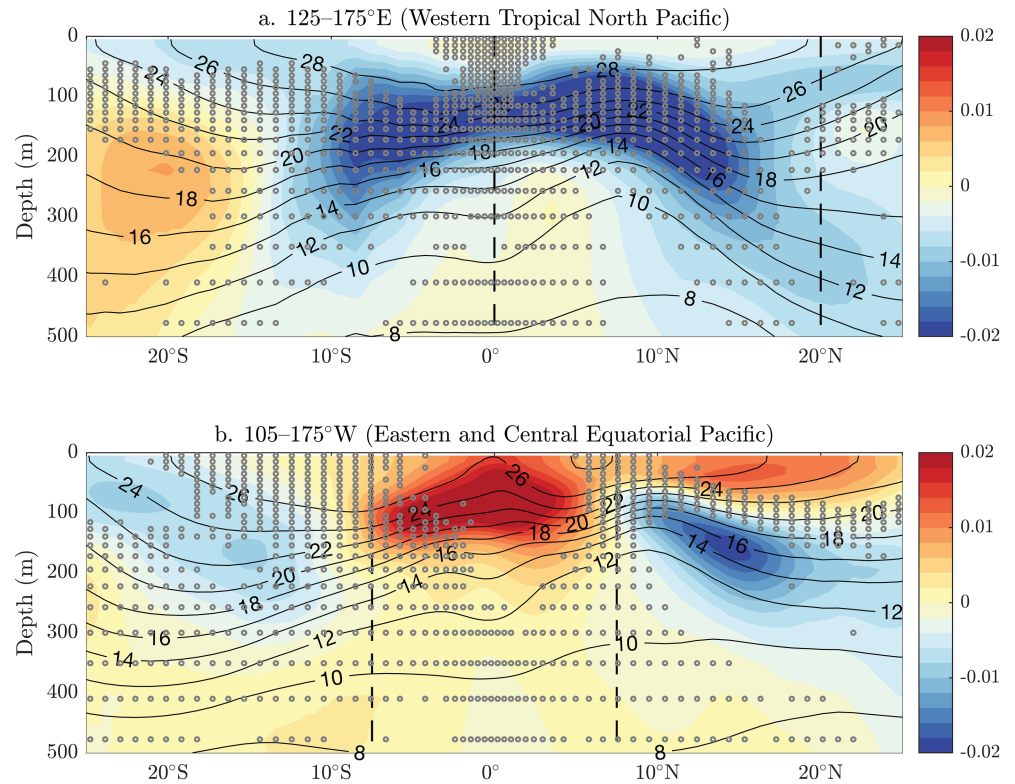


Figure 4. Shading represents accelerations (positive, warm colors) and decelerations (negative, cool colors) in θ over 1993–2015 averaged zonally across the (a) WTNP and (b) ECEP from ECCOv4 ($^{\circ}\text{C}/\text{year}^2$). Thick black solid contours mark zonally and temporally averaged isotherms. Thin black dashed vertical lines mark the latitudinal bounds of the two study regions. Gray dots indicate where values are not statistically significant at the $p = 0.10$ level.

the buoyancy fluxes are specified separately from the wind stresses used in the momentum flux, and identical wind speeds are used for both the ECCOv4 setup and the perturbation experiment. Momentum forcing by anomalous wind stress could thus cause θ_0 changes that, all else being equal, would cause heat-flux anomalies at the surface and related $\zeta_T^{\prime\prime}$ changes.

We use model output to comprehensively quantify $\zeta_T^{\prime\prime}$ contributions from internal ocean transports and external surface exchanges (Piecuch & Ponte, 2011). Based on the heat conservation equation, we decompose $\zeta_T^{\prime\prime}$ into contributions from advection by large-scale ocean circulation $\mathcal{A}^{\prime\prime}$, diffusion by parameterized small-scale mixing $\mathcal{M}^{\prime\prime}$, and local forcing by radiative and turbulent surface heat fluxes $\mathcal{F}^{\prime\prime}$ (see Appendix A),

$$\zeta_T^{\prime\prime} = \mathcal{A}^{\prime\prime} + \mathcal{M}^{\prime\prime} + \mathcal{F}^{\prime\prime}. \quad (3)$$

All terms are diagnosed independently, and the budget closes exactly (cf. Piecuch, 2017).

Figure 6 shows $\zeta_T^{\prime\prime}$ budget time series averaged across the WTNP and ECEP. The regional $\zeta_T^{\prime\prime}$ balance is complex, and $\zeta_T^{\prime\prime}$ changes are not simply determined by $\mathcal{A}^{\prime\prime}$ changes in all cases, as would be anticipated if adiabatic redistribution by ocean circulation were the only relevant process. Rather, changes in $\zeta_T^{\prime\prime}$ result from the subtle interweaving of $\mathcal{A}^{\prime\prime}$ and $\mathcal{F}^{\prime\prime}$ effects, such that the dominant balance depends on frequency band and region. Contributions from $\mathcal{A}^{\prime\prime}$ seem most influential on shorter, intraseasonal to interannual time scales, whereas $\mathcal{F}^{\prime\prime}$ impacts become increasingly important at longer, decadal periods. Impacts of $\mathcal{M}^{\prime\prime}$ are negligible on all time sales.

These conclusions, based on inspection of $\zeta_T^{\prime\prime}$ budgets in the time domain, are corroborated by power spectral density estimates in frequency space (Figure 7). All budget terms show increasing power at decreasing frequency. In both regions, advection is important at all time scales, and $\zeta_T^{\prime\prime}$ and $\mathcal{A}^{\prime\prime}$ show similar power spectral densities over most frequency bands (Figures 7a and 7b). Forcing grows more influential at decreasing frequency in both the WTNP and ECEP, but $\mathcal{F}^{\prime\prime}$ effects on $\zeta_T^{\prime\prime}$ changes are relatively more important in

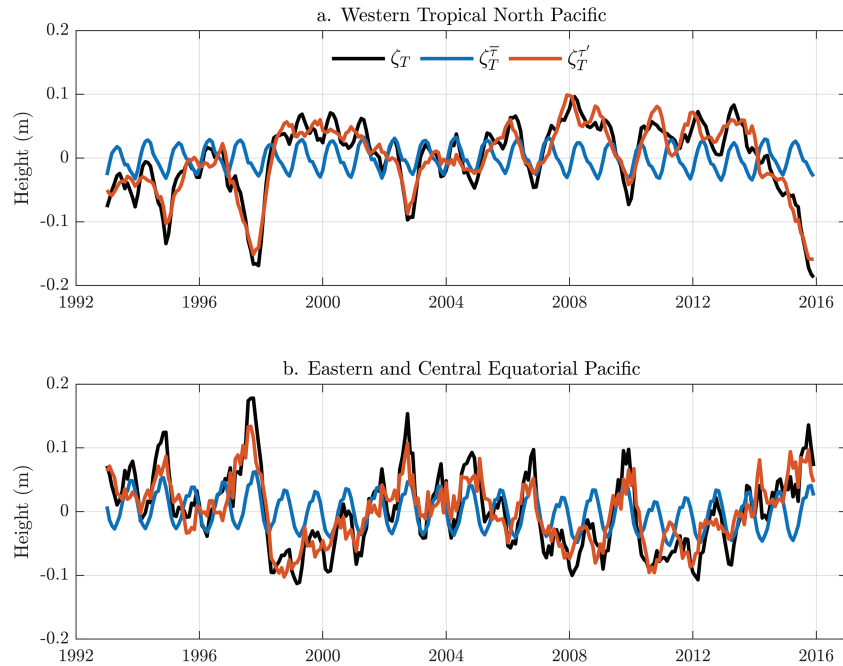


Figure 5. Decomposition of ζ_T (black) into contributions from climatological wind-stress forcing ζ_T^c (blue) and anomalous wind-stress forcing ζ_T^a (orange) averaged over the (a) WTNP and (b) ECEP from ECCOV4. See equation (2) for breakdown.

the ECEP compared to the WTNP for a given frequency band (Figures 7c and 7d). For example, at ~ 5 -year periods, the ratio of $\mathcal{F}^{r'}$ to $\zeta_T^{r'}$ power spectral densities is ~ 0.8 in the ECEP (Figure 7d) but only ~ 0.2 in the WTNP (Figure 7c). Inspecting phase relationships from an admittance and coherence analysis (not shown), we find that $\zeta_T^{r'}$ and $\mathcal{F}^{r'}$ are roughly in quadrature (i.e., $\sim 90^\circ$ out of phase, such that $\mathcal{F}^{r'}$ leads $\zeta_T^{r'}$) in both regions on interannual to decadal time scales, suggesting that $\mathcal{F}^{r'}$ acts to damp the $\zeta_T^{r'}$ changes.

At the lowest frequencies, $\mathcal{F}^{r'}$ becomes especially important to the $\zeta_T^{r'}$ budget (Figure 6). In the WTNP, $\mathcal{F}^{r'}$ accounts for 96% of the magnitude of the significant deceleration in $\zeta_T^{r'}$ (Table 1). A compensating deceleration in $\mathcal{A}^{r'}$ partly alleviates the $\mathcal{F}^{r'}$ impacts on the $\zeta_T^{r'}$ acceleration in the ECEP, such that $\mathcal{F}^{r'}$ amounts to 181% of the amplitude of the significant acceleration in $\zeta_T^{r'}$ in that region (Table 1). While $\mathcal{F}^{r'}$ accelerations and decelerations are not significant at the $p \leq 0.10$ level, accelerations and decelerations in $\mathcal{A}^{r'}$ and $\mathcal{M}^{r'}$ have smaller magnitudes and are less statistically significant (Table 1).

This budget analysis corroborates past studies emphasizing the role of wind-driven internal redistribution, in the sense that large-scale advective transports are confirmed to be important (e.g., McGregor et al., 2012; Merrifield, 2011; Timmermann et al., 2010). However, it also reveals that other effects not typically discussed, namely, diabatic local surface heat fluxes (cf. Fukumori & Wang, 2013), are involved and become increasingly relevant at low frequency.

3.4. Nature of $\mathcal{F}^{r'}$

Wind stress does not directly effect local surface heat flux in the model, in that it does not appear in the bulk formulae. However, wind stress has a potential indirect influence, insofar as it drives changes in θ_0 , which do appear in the bulk formulae (e.g., Large & Yeager, 2004, section 2). Since all other atmospheric state variables (temperature, humidity, radiation, precipitation, etc.) used in the surface boundary conditions are identical in the ECCOV4 setup and the perturbation experiment, the $\mathcal{F}^{r'}$ contributions to the $\zeta_T^{r'}$ changes in the WTNP and ECEP should mainly relate to differences in θ_0 between the two simulations arising from the presence or absence of anomalous wind-stress forcing.

To clarify the nature of the $\mathcal{F}^{r'}$ effects on the $\zeta_T^{r'}$ changes, we partition the former into contributions from latent $\mathcal{F}_E^{r'}$, sensible $\mathcal{F}_H^{r'}$, longwave $\mathcal{F}_L^{r'}$, and shortwave $\mathcal{F}_S^{r'}$ heat fluxes, and the heat transfer associated with surface freshwater exchanges $\mathcal{F}_P^{r'}$ (see Appendix A),

$$\mathcal{F}^{r'} = \mathcal{F}_E^{r'} + \mathcal{F}_H^{r'} + \mathcal{F}_S^{r'} + \mathcal{F}_L^{r'} + \mathcal{F}_P^{r'}. \quad (4)$$

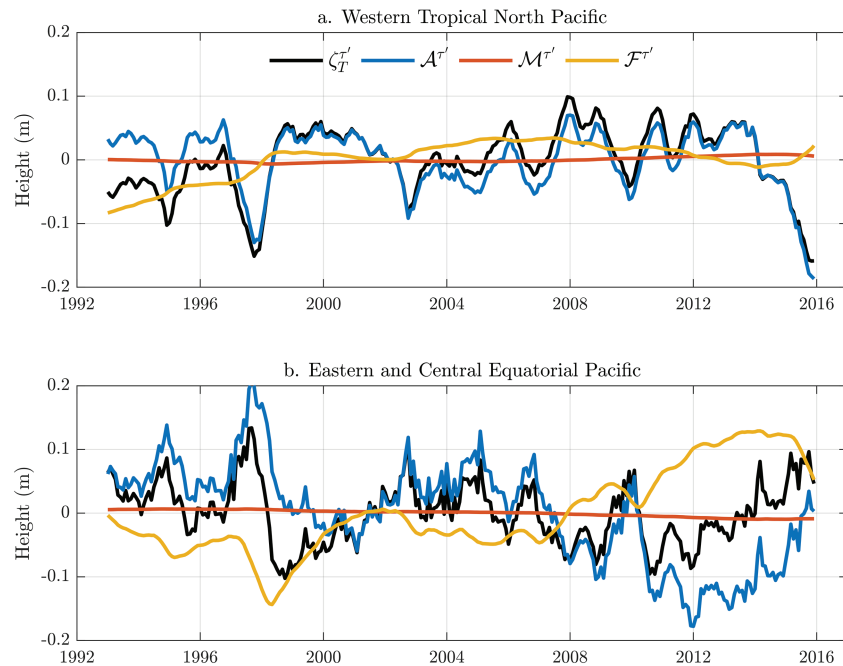


Figure 6. Decomposition of $\zeta_T^{r'}$ (black) into contributions from large-scale advection $\mathcal{A}^{r'}$ (blue), small-scale mixing $\mathcal{M}^{r'}$ (orange), and sea-surface forcing $\mathcal{F}^{r'}$ (yellow) averaged over the (a) WTNP and (b) ECEP from ECCOv4. See equation (3) for breakdown.

All terms in the $\mathcal{F}^{r'}$ budget are diagnosed independently using model output.

Figure 8 breaks down the $\mathcal{F}^{r'}$ time series into their constituent parts. Latent heat fluxes $\mathcal{F}_E^{r'}$ contribute most importantly to the surface heat exchanges $\mathcal{F}^{r'}$ in the WTNP and ECEP: $\mathcal{F}_E^{r'}$ explains $\sim 90\%$ of the total monthly variance and $\sim 75\%$ of the acceleration or deceleration in $\mathcal{F}^{r'}$ in both regions (cf. Table 1). Sensible and longwave components make secondary contributions to the $\mathcal{F}^{r'}$ budget. Local surface heat fluxes related to shortwave radiation and precipitation are comparatively less important, though not identically zero. (Nonzero contributions from $\mathcal{F}_S^{r'}$ and $\mathcal{F}_P^{r'}$ are not rendered directly by shortwave radiation and precipitation, which are identical between the ECCOv4 solution and the perturbation experiment, but instead by differences between the two experiments in terms of thermal expansion coefficients, which are nonlinear functions of the background temperature field.) The $\mathcal{F}_E^{r'}$ changes are determined by a nonlinear function of surface atmospheric specific humidity, θ_0 (through its influence on specific humidity at saturation), and wind speed (cf. equation 4 in Large & Yeager, 2004). Closer inspection of model output (not shown) demonstrates that the $\mathcal{F}_E^{r'}$ changes in both study regions are wholly due to θ_0 effects alone, not nonlinear products involving atmospheric specific humidity or wind speed changes, consistent with our earlier intuition.

4. Discussion

Satellite altimetry reveals substantial decadal variability in sea level ζ across the tropical Pacific during 1993–2015 (Figure 1). We used an ocean state estimate that faithfully reproduces the observations (Figure 2) to elucidate low-frequency ζ changes over the tropical Pacific, focusing on the western tropical North Pacific (WTNP) and eastern and central equatorial Pacific (ECEP) regions (cf. Figure 1). Analysis of the hydrostatic equation showed that recent decadal ζ changes in the WTNP and ECEP are mainly thermosteric in nature (Figure 3), related to changes in upper-ocean heat content (Figure 4). A forcing experiment performed with the numerical model revealed that the relevant heat storage and thermosteric variation arose from shifts in the overlying wind-stress field (Figure 5). Closed budget diagnostics further clarify that the wind-stress-related thermosteric ζ variation resulted from the joint actions of large-scale ocean advection and local surface heat flux (Figure 6), such that advection controlled the budget over shorter, intraseasonal to interannual time scales, and local surface heat flux became increasingly important at longer decadal periods (Figure 7). In particular, local surface heat flux was important in contributing to a recent reversal of decadal ζ trends in the tropical Pacific (Table 1). Contributions from local surface heat flux partly

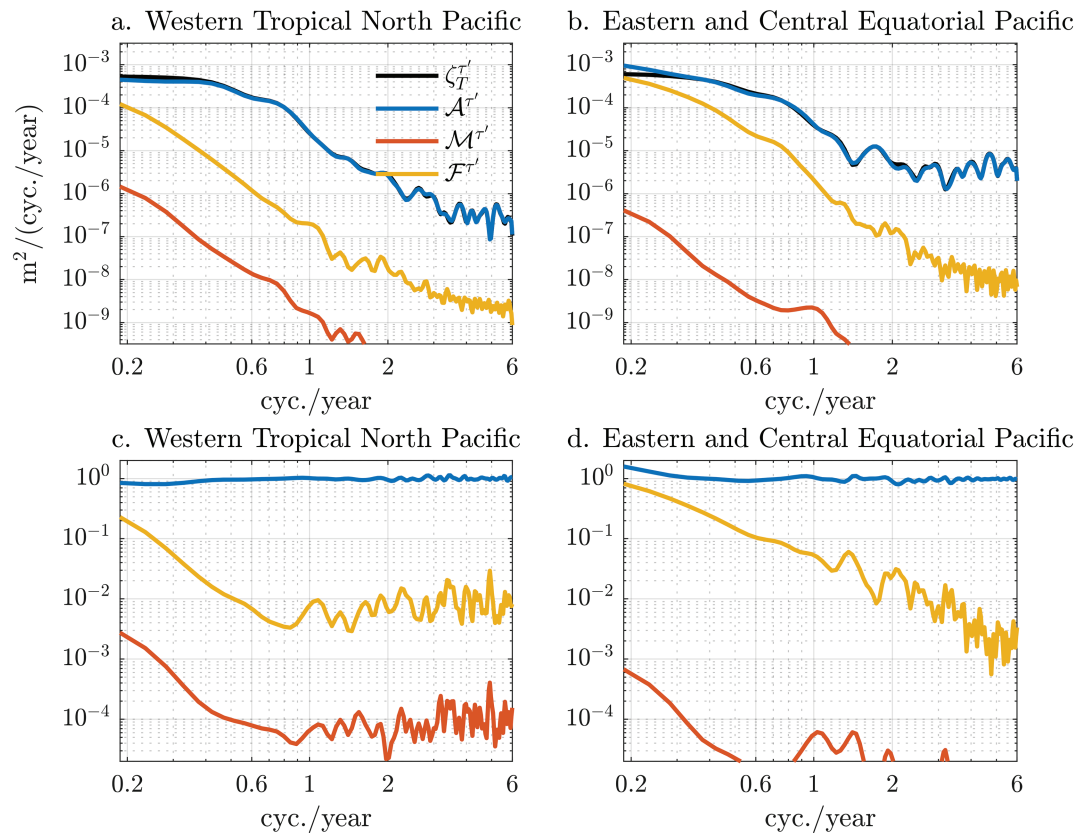


Figure 7. Power spectral density estimates of $\zeta_T^{r'}$ (black) and contributions from large-scale advection $\mathcal{A}^{r'}$ (blue), small-scale mixing $\mathcal{M}^{r'}$ (orange), and sea-surface forcing $\mathcal{F}^{r'}$ (yellow) over the (a) WTNP and (b) ECEP from ECCOv4. Panels (c) and (d) are as in (a) and (b), but the regional advection, mixing, and forcing power spectral densities are divided by the $\zeta_T^{r'}$ power spectral density for that region. See equation (3) for breakdown.

reflect damping latent (evaporative) heat exchanges related to wind-stress-driven sea-surface-temperature variations (Figure 8).

Our results build on previous works. Most past studies interpreted observed ζ patterns in the tropical Pacific in terms of adiabatic internal redistribution of ocean heat content due to shifts in the overlying wind field (McGregor et al., 2012; Merrifield, 2011; Merrifield & Maltrud, 2011; Merrifield et al., 2012; Moon & Song, 2013; Moon et al., 2013; Qiu & Chen, 2012; Timmermann et al., 2010). We showed that, added to the effects of ocean heat transport by large-scale advective processes, local sea-surface heat exchanges also contributed to the ζ changes seen in the altimeter record, especially at the lowest frequencies.

The importance of local surface heat fluxes was overlooked in the past perhaps because most previous analyses were based on qualitative comparisons to simplified ocean model frameworks (e.g., McGregor et al., 2012; Qiu & Chen, 2012; Timmermann et al., 2010) or corresponding shifts observed in the prevailing winds (e.g., Merrifield, 2011). Using a non-Boussinesq global ocean general circulation model, Moon and Song (2013) reasoned that local surface heat flux was unimportant to low-frequency changes in ocean heat content and ζ in the North Equatorial Current region of the WTNP during 1993–2010. This reasoning does not conflict with our results, which highlight the importance of local surface heat flux, since Moon and Song (2013) performed their budget analysis in time-tendency space and considered all nonseasonal time scales collectively. Thus, their results emphasized the more pronounced interannual ζ variations tied to advection and understated the subtler decadal ζ changes due to local surface heat flux relative to our findings, which are based on a time-integrated budget analysis particularly focused on long-term behavior.

Our findings, based on a quantitative diagnosis of a general circulation model fit to most available ocean data, corroborate the modeling results of Fukumori and Wang (2013), who performed passive tracer experiments using an earlier global ocean state estimate. They argued that surface heat fluxes contributed importantly to

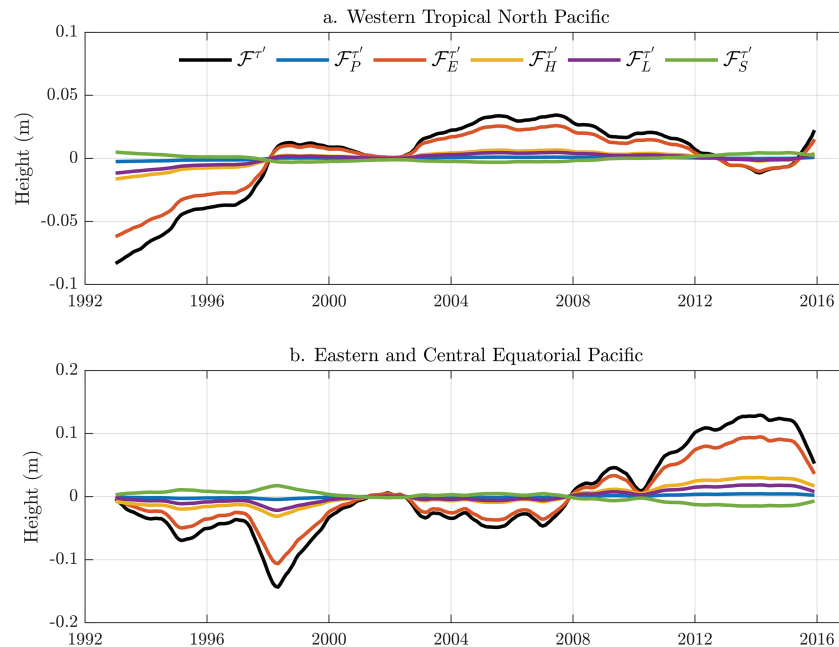


Figure 8. Decomposition of $F^{T'}$ (black) into contributions from precipitation $F_P^{T'}$ (blue), latent $F_E^{T'}$ (orange), sensible $F_H^{T'}$ (yellow), longwave $F_L^{T'}$ (purple), and shortwave $F_S^{T'}$ (green) heat fluxes averaged over the (a) WTNP and (b) ECEP from ECCOv4. See Equation (4) for breakdown.

ζ patterns observed by altimetry over the western tropical Pacific during the shorter 1993–2004 period. Our results are also consistent with the literature on the surface warming slowdown emphasizing the importance of coupling and sea-surface exchanges to the evolution of the ocean-atmosphere system in the Pacific during recent decades (Delworth et al., 2015; England et al., 2014; Kosaka & Xie, 2013; McGregor, 2014; Meehl et al., 2013; Watanabe et al., 2014).

We should acknowledge some caveats and outstanding questions prompted by our analysis but beyond our scope to address. The end of our study period (1993–2015) coincides with the strong El Niño event during 2014–2016 (e.g., Parker et al., 2016). It is possible that some of our results (e.g., acceleration and deceleration statistics in Table 1) are subject to end effects related to the anomalously warm conditions over the ECEP and cool conditions across the WTNP during this time. We therefore emphasize that our results should be taken to apply strictly to the study period. Future investigations of other periods (e.g., based on an updated state estimate covering a longer time period) should be performed to understand the nature of decadal ζ variability in the tropical Pacific, and the competing effects of large-scale ocean advection and local surface heat fluxes, more generally.

Uncertainty estimates given here (e.g., Table 1) are formal errors based on the spectral properties of residual time series. They do not account for possible systematic errors and should be interpreted as conservative lower bounds on the true uncertainties. The atmospheric boundary conditions used to generate the ocean model solutions studied here are based on a particular atmospheric reanalysis product (Dee et al., 2011). However, atmospheric reanalysis surface products have uncertainties that, when applied as boundary conditions, can lead to differences in ocean model solutions (Chaudhuri et al., 2016; Merrifield & Maltrud, 2011; McGregor et al., 2012; Pillar et al., 2018). While surface heat fluxes from ECCOv4 and OAFflux (Yu & Weller, 2007) show good agreement over the WTNP and ECEP (Figures S15 and S16), subtle distinctions between the two at low frequencies translate to important differences in terms of decadal variability in heat content and ζ (Figure S17). A future study should quantify the sensitivity of our results to atmospheric uncertainties (including the impact of the adjustments made to the first-guess atmospheric fields as part of the state estimation) by performing additional experiments using different atmospheric reanalysis products for the surface boundary conditions.

We found that local surface-heat-flux forcing, which appears to damp ζ changes, operates on different time scales in the two study regions, being relatively more important at higher frequencies in the ECEP compared

to the WTNP (Figures 6 and 7). However, it was unclear what sets the distinct dependences on time scale in the two regions. Perhaps there are connections to vertical structure and surface-subsurface coupling, such that the relatively more surface-intensified temperature changes in the ECEP allow more ready communication with the atmosphere compared to the WTNP (cf. Figure 4). Regional differences in terms of overall sea-surface-temperature variability or background-mean thermocline depth are also potentially relevant in this context (e.g., Deser et al., 2010; Frankignoul & Hasselmann, 1977). Resolving this issue could aid coupled climate model simulations, which underestimate the magnitude of tropical Pacific decadal ζ variability (Peysner & Yin, 2017).

Our goal was to identify the role and elucidate the nature of local surface heat fluxes. We did not interrogate the nature of advection contributions to the budget (Figure 6). These changes can arise from anomalous flows acting on background temperatures, mean currents transporting anomalous temperatures, or covariation between temperatures and velocities. Moreover, the wind-stress-related advection diagnosed here (Figure 6) need not be entirely adiabatic and momentum driven, since surface heat fluxes differ between the two model experiments. Using an earlier state estimate to study interannual ζ changes in the tropical South Atlantic, Piecuch and Ponte (2013) found that local surface heat fluxes excite a dynamic ζ adjustment mediated by planetary waves. Such a dynamic ζ response to surface heat flux would manifest in the advection term in equation (3), grouped alongside the effects of heat transport and adiabatic redistribution related to momentum input from wind stress (cf. Piecuch & Ponte, 2013). A more detailed study of the advection, quantifying velocity and temperature effects driven by buoyancy flux and momentum input, is warranted to clarify of our results.

We assumed that the effects of different surface atmospheric variables on the ocean are linear and separable, and so we interpreted ζ differences between model experiments as resulting from anomalous wind stress. However, we acknowledge that this assumption likely does not hold strictly and that differences in ζ between the two model experiments could also arise from nonlinear, inseparable ocean response to surface atmospheric variation. Piecuch and Ponte (2012) quantified the influence of nonlinear effects on interannual ζ variability during 1993–2004 in the tropical South Pacific based on an earlier state estimate. That study showed that while less important than direct forcing by wind stress and buoyancy flux, such complex nonlinear processes are not negligible for a comprehensive, quantitative description of ζ changes. In the future, to quantify any nonlinearities in the ocean's response, a broader suite of target forcing perturbation experiments should be performed, similar to Yeager and Danabasoglu (2014).

Due to space considerations, we did not study ζ changes over the coastal northeast Pacific Ocean, off the coast of southern California, and the Gulf of Alaska, which also show substantial decadal ζ variability in the altimeter data during 1993–2015 (Figure 1). To what extent are the processes highlighted here for the tropics relevant for these other coastal or midlatitude areas? Future studies could investigate the physics of decadal ζ variation in these regions.

Finally, the local surface heat fluxes identified here, driven by sea-surface temperatures, imply an atmospheric-circulation response (e.g., Gill, 1980). Due to the nature of our model (ocean only with a prescribed atmosphere), we were precluded from studying the attendant atmospheric response and its associated time scales. Given the importance of understanding the dynamics of the coupled atmosphere-ocean system, such outstanding questions should be addressed in future work.

Appendix A: Formulation of the Thermosteric-Height Budget Using a Scaled Vertical Coordinate (z^*)

Building on work by Piecuch and Ponte (2011), we formulate the thermosteric-height budget for the rescaled height coordinate z^* used in the ECCOV4 governing equations,

$$z^* = \frac{z - \eta(x, y, t)}{H(x, y) + \eta(x, y, t)} H(x, y), \quad (\text{A1})$$

where z is the unscaled vertical coordinate, $\eta(x, y, t)$ is the spatiotemporally variable height of the sea surface (distinct from ζ as described below), $H(x, y)$ is the spatially variable ocean depth, x and y are the horizontal coordinates, and t is time (Adcroft & Campin, 2004). The range of the scaled height coordinate is $z^* \in [-H, 0]$; though the physical free surface moves, the upper boundary in the z^* frame does not vary in time (Adcroft & Campin, 2004).

In the z^* frame, the hydrostatic equation is given as

$$\left(\frac{H+\eta}{H}\right)g\rho + \partial_{z^*}p = 0, \quad (\text{A2})$$

where g is gravity, ρ total density, p hydrostatic pressure, and ∂_{z^*} is the vertical divergence in the z^* frame (see section 2 in Adcroft & Campin, 2004). After Gill and Niiler (1973), we partition the density as

$$\rho(x, y, z^*, t) = \rho_0 + \rho'(x, y, z^*, t), \quad (\text{A3})$$

such that $\rho_0 \gg \rho'$. Then, we integrate the hydrostatic balance over the range of the scaled vertical coordinate, drop a term that is constant in time, divide by the constant value $\rho_0 g$, and rearrange the resulting expression to give

$$\eta + \frac{p(z^* = 0)}{\rho_0 g} = -\frac{1}{\rho_0} \frac{H+\eta}{H} \int_{-H}^0 \rho' dz^* + \frac{p(z^* = -H)}{\rho_0 g}. \quad (\text{A4})$$

The term of the left-hand side is the effective sea level ζ , that is, the physical deviation of the sea surface itself, along with the effects of surface loading (due to pressure forcing or sea ice). The second term on the right-hand side reflects net changes in the mass of the water column ζ_M (associated with bottom pressure). The first term on the right-hand side is the steric height ζ_ρ . Note that the definition

$$\zeta_\rho \doteq -\frac{1}{\rho_0} \frac{H+\eta}{H} \int_{-H}^0 \rho' dz^* \quad (\text{A5})$$

is distinct from definitions of steric height in the literature based on the primitive equations in an unscaled height coordinate (Gill & Niiler, 1973; Griffies & Greatbatch, 2012) in that a factor appears before the integral that accounts for stretching and squashing of the water column.

Taking the derivative of equation (A5) and using the product rule gives

$$\frac{\partial \zeta_\rho}{\partial t} = -\frac{1}{\rho_0} \left(\frac{1}{H} \frac{\partial \eta}{\partial t} \int_{-H}^0 \rho' dz^* + \frac{H+\eta}{H} \int_{-H}^0 \frac{\partial \rho'}{\partial t} dz^* \right). \quad (\text{A6})$$

This expression shows that ζ_ρ changes arise both from changes in the sea level at constant density (first term) and from changes in the density at constant sea level (second term). Given a nonlinear seawater equation of state $\rho' = \rho'(\theta, S, p_0)$, where S is salinity and p_0 is a reference pressure, the product and chain rules result in the following expression:

$$\begin{aligned} \frac{\partial \zeta_\rho}{\partial t} = & -\frac{1}{\rho_0} \int_{-H}^0 \left[\frac{\partial \rho'}{\partial \theta} \frac{\partial}{\partial t} \left(\frac{H+\eta}{H} \theta \right) + \frac{\partial \rho'}{\partial S} \frac{\partial}{\partial t} \left(\frac{H+\eta}{H} S \right) \right. \\ & \left. + \frac{1}{H} \frac{\partial \eta}{\partial t} \left(\rho' - \frac{\partial \rho'}{\partial \theta} \theta - \frac{\partial \rho'}{\partial S} S \right) \right] dz^*. \end{aligned} \quad (\text{A7})$$

The first term under the integral on the right-hand side relates to thermosteric changes ζ_T due to changes in heat content, whereas the second term under the integral on the right-hand side relates to halosteric changes ζ_S due to changes in salt content. The final term under the integral on the right-hand side corresponds to a correction term ζ_N that appears in consequence of the nonlinear free-surface boundary condition in combination with a nonlinear equation of state. Combining equations (A5) and (A7) thus gives

$$\frac{\partial \zeta}{\partial t} = \frac{\partial \zeta_T}{\partial t} + \frac{\partial \zeta_S}{\partial t} + \frac{\partial \zeta_N}{\partial t} + \frac{\partial \zeta_M}{\partial t}, \quad (\text{A8})$$

which is the time derivative form of the hydrostatic decomposition (equation (1)) given in the main text.

In ECCOV4, the heat conservation equation is

$$\frac{\partial}{\partial t} \left(\frac{H+\eta}{H} \theta \right) + \nabla_{z^*} \cdot \left(\frac{H+\eta}{H} \theta \vec{v}_{res} \right) + \frac{\partial (\theta w_{res})}{\partial z^*} = \frac{H+\eta}{H} F_\theta + \frac{H+\eta}{H} (D_{\parallel, \theta} + D_{\perp, \theta}), \quad (\text{A9})$$

where (\vec{v}_{res}, w_{res}) is the residual-mean velocity, ∇_{z^*} is the nabla operator at constant z^* , F_θ is the forcing term (generally concentrated at the surface but also including a temporally constant geothermal flux at the

seafloor), and $D_{\parallel,\theta}$ and $D_{\perp,\theta}$ are, respectively, dia-neutral and iso-neutral subgrid-scale mixing effects (Forget et al., 2015). Thus, combining the definition of ζ_T in equation (A7) with the heat balance in equation (A9) gives

$$\frac{\partial \zeta_T}{\partial t} = -\frac{1}{\rho_0} \int_{-H}^0 \left\{ \frac{\partial \rho'}{\partial \theta} \left[\left\langle -\nabla_{z^*} \left(\frac{H+\eta}{H} \theta \bar{v}_{res} \right) - \frac{\partial (\theta w_{res})}{\partial z^*} \right\rangle + \left\langle \frac{H+\eta}{H} F_\theta \right\rangle + \left\langle \frac{H+\eta}{H} (D_{\parallel,\theta} + D_{\perp,\theta}) \right\rangle \right] \right\} dz^* \quad (\text{A10})$$

The first angle-bracketed term on the right-hand side corresponds to the time derivative of the advection term \mathcal{A} , the second bracketed term on the right-hand side the time derivative of the forcing term \mathcal{F} , and the third bracketed term on the right-hand side the time derivative of the mixing term \mathcal{M} in the ζ_T budget. Equation (A10) is equivalent to a time derivative form of equation (3) used in the main text.

The surface forcing F_θ in the heat budget comprises several components:

$$F_\theta = F_{\theta,E} + F_{\theta,H} + F_{\theta,S} + F_{\theta,L} + F_{\theta,P}, \quad (\text{A11})$$

where subscripts E , H , S , L , and P denote latent (evaporative), sensible, shortwave, longwave, and precipitation contributions to the total heat flux, respectively. (Note that we ignore a time-constant geothermal flux at the seafloor.) Thus, the contribution of any one heat flux component to the ζ_T budget can be written as

$$\frac{\partial F_\alpha}{\partial t} = -\frac{1}{\rho_0} \int_{-H}^0 \left\{ \frac{\partial \rho'}{\partial \theta} \left(\frac{H+\eta}{H} F_{\theta,\alpha} \right) \right\} dz^*, \quad (\text{A12})$$

where $\alpha \in \{E, H, S, L, P\}$ (cf. equation (4) in the main text).

Acknowledgments

This work was supported by NSF Awards OCE-1558966 and OCE-1834739. Support of the ECCO project by the NASA Physical Oceanography, Cryospheric Science, and Modeling, Analysis and Prediction programs is also acknowledged. We thank Ou Wang (NASA JPL) for performing the forcing perturbation experiment. Comments from two anonymous reviewers were helpful. Altimetry observations used in Figures 1 and 2 were downloaded from CSIRO (<http://www.cmar.csiro.au/sealevel/sl&urlscore;data&urlscore;cmr.html>). ECCOV4 output is available on the group website (<https://ecco.jpl.nasa.gov/>).

References

- Adcroft, A., & Campin, J.-M. (2004). Rescaled height coordinates for accurate representation of free-surface flows in ocean circulation models. *Ocean Modelling*, 7, 269–284. <https://doi.org/10.1016/j.ocemod.2003.09.003>
- Ando, K., & Kuroda, Y. (2002). Two models of salinity and temperature variation in the surface layer of the Pacific Warm Pool. *Journal of Oceanography*, 58, 599–609. <https://doi.org/10.1023/A:1021223028579>
- Bonjean, F., & Lagerloef, G. S. E. (2002). Diagnostic model and analysis of the surface currents in the Tropical Pacific Ocean. *Journal of Physical Oceanography*, 32, 2938–2954. [https://doi.org/10.1175/1520-0485\(2002\)032<2938:DMAAOT>2.0.CO;2](https://doi.org/10.1175/1520-0485(2002)032<2938:DMAAOT>2.0.CO;2)
- Bos, M. S., Williams, S. D. P., Araújo, I. B., & Bastos, L. (2014). The effect of temporal correlated noise on the sea level rate and acceleration uncertainty. *Geophysical Journal International*, 196, 1423–1430. <https://doi.org/10.1093/gji/ggt481>
- Cazenave, A., & Llovel, W. (2010). Contemporary sea level rise. *Annual Review of Marine Science*, 2, 145–173. <https://doi.org/10.1146/annurev-marine-120308-081105>
- Cazenave, A., Palanisamy, H., & Ablain, M. (2018). Contemporary sea level changes from satellite altimetry: What have we learned? What are the new challenges? *Advances in Space Research*, 62, 1639–1653. <https://doi.org/10.1016/j.asr.2018.07.017>
- Chaudhuri, A. H., Ponte, R. M., & Forget, G. (2016). Impact of uncertainties in atmospheric boundary conditions on ocean model solutions. *Ocean Modelling*, 100, 96–108. <https://doi.org/10.1016/j.ocemod.2016.02.003>
- Cheng, W., McPhaden, M. J., Zhang, D., & Metzger, E. J. (2007). Recent changes in the Pacific subtropical cells inferred from an eddy-resolving ocean circulation model. *Journal of Physical Oceanography*, 37, 1340–1356. <https://doi.org/10.1175/JPO3051.1>
- Church, J. A., & White, N. J. (2011). Sea-level rise from the late 19th to the early 21st century. *Surveys in Geophysics*, 32, 585–602. <https://doi.org/10.1007/s10712-011-9119-1>
- Dee, D. P., Dee, D. P., Uppala, S. M., Simmons, A. J., Berrisford, P., Poli, P., et al. (2011). The ERA-Interim reanalysis: Configuration and performance of the data assimilation system. *Quarterly Journal of the Royal Meteorological Society*, 137, 553–597. <https://doi.org/10.1002/qj.828>
- Delworth, T. L., Zeng, F., Rosati, A., Vecchi, G. A., & Wittenberg, A. T. (2015). A link between the hiatus in global warming and North American drought. *Journal of Climate*, 28, 3834–3845. <https://doi.org/10.1175/JCLI-D-14-00616.1>
- Deser, C., Alexander, M. A., Xie, S.-P., & Phillips, A. S. (2010). Sea surface temperature variability: Patterns and mechanisms. *Annual Reviews of Marine Science*, 2, 115–143. <https://doi.org/10.1146/annurev-marine-120408-151453>
- England, M. H., McGregor, S., Spence, P., Meehl, G. A., Timmermann, A., Cai, W., et al. (2014). Recent intensification of wind-driven circulation in the Pacific and the ongoing warming hiatus. *Nature Climate Change*, 4, 222–227. <https://doi.org/10.1038/nclimate2106>
- Feng, M., McPhaden, M. J., & Lee, T. (2010). Decadal variability of the Pacific subtropical cells and their influence on the southeast Indian Ocean. *Geophysical Research Letters*, 37, L09606. <https://doi.org/10.1029/2010GL042796>
- Forget, G., Campin, J.-M., Heimbach, P., Hill, C. N., Ponte, R. M., & Wunsch, C. (2015). ECCO version 4: An integrated framework for non-linear inverse modeling and global ocean state estimation. *Geoscientific Model Development*, 8, 3071–3104. <https://doi.org/10.5194/gmd-8-3071-2015>
- Forget, G., & Ponte, R. M. (2015). The partition of regional sea level variability. *Progress in Oceanography*, 137, 173–195. <https://doi.org/10.1016/j.pocean.2015.06.002>
- Frankignoul, C., & Hasselmann, K. (1977). Stochastic climate models. Part 2. Application to sea-surface temperature variability and thermocline variability. *Tellus*, 29, 285–305. <https://doi.org/10.1111/j.2153-3490.1977.tb00740.x>
- Fukumori, I., Fenty, I., Forget, G., Heimbach, P., King, C., Nguyen, A. T., et al. (2018). Data sets used in ECCO Version 4 Release 3. Retrieved from <https://dspace.mit.edu/handle/1721.1/120472>

- Fukumori, I., & Wang, O. (2013). Origins of heat and freshwater anomalies underlying regional decadal sea level trends. *Geophysical Research Letters*, *40*, 563–567. <https://doi.org/10.1002/grl.50164>
- Fukumori, I., Wang, O., Fenty, I., Forget, G., Heimbach, P., & Ponte, R. M. (2017). *ECCO Version 4 Release 3*. Pasadena, CA: Jet Propulsion Laboratory. Retrieved from <http://hdl.handle.net/1721.1/110380>, ftp://ecco.jpl.nasa.gov/Version4/Release3/doc/v4r3_estimation_synopsis.pdf
- Fyfe, J. C., Meehl, G. A., England, M. H., Mann, M. E., Santer, B. D., Flato, G. M., et al. (2016). Making sense of the early-2000s warming slowdown. *Nature Climate Change*, *6*, 224–227. <https://doi.org/10.1038/nclimate2938>
- Gaspar, P., Grégoris, Y., & Lefevre, J.-M. (1990). A simple eddy kinetic energy model for simulations of the oceanic vertical mixing: Tests at Station Papa and long-term upper ocean study site. *Journal of Geophysical Research*, *95*, 16,179–16,193. <https://doi.org/10.1029/JC095iC09p16179>
- Gent, P. R., & McWilliams, J. C. (1990). Isopycnal mixing in ocean circulation models. *Journal of Physical Oceanography*, *20*, 150–155. [https://doi.org/10.1175/1520-0485\(1990\)020<0150:IMIOCM>2.0.CO;2](https://doi.org/10.1175/1520-0485(1990)020<0150:IMIOCM>2.0.CO;2)
- Gill, A. E. (1980). Some simple solutions for heat-induced tropical circulation. *Quarterly Journal of the Royal Meteorological Society*, *106*, 447–462. <https://doi.org/10.1002/qj.49710644905>
- Gill, A. E., & Niiler, P. P. (1973). The theory of the seasonal variability in the ocean. *Deep Sea Research and Oceanographic Abstracts*, *20*(2), 141–177. [https://doi.org/10.1016/0011-7471\(73\)90049-1](https://doi.org/10.1016/0011-7471(73)90049-1)
- Griffies, S. M., & Greatbatch, R. J. (2012). Physical processes that impact the evolution of global mean sea level in ocean climate models. *Ocean Modelling*, *51*, 37–72. <https://doi.org/10.1016/j.ocemod.2012.04.003>
- Hamlington, B. D., Cheon, S. H., Thompson, P. R., Merrifield, M. A., Nerem, R. S., Leben, R. R., & Kim, K.-Y. (2016). Journal of geophysical research: Oceans, *121*, 5084–5097. <https://doi.org/10.1002/2016JC011815>
- Karl, T. R., Arguez, A., Huang, B., Lawrimore, J. H., McMahon, J. R., Menne, M. J., et al. (2015). Possible artifacts of data biases in the recent global surface warming hiatus. *Science*, *348*, 1469–1472. <https://doi.org/10.1126/science.aaa5632>
- Kosaka, Y., & Xie, S.-P. (2013). Recent global-warming hiatus tied to equatorial Pacific surface cooling. *Nature*, *501*, 403–407. <https://doi.org/10.1038/nature12534>
- Large, W. G., & Yeager, S. (2004). Diurnal to decadal global forcing for ocean and sea-ice models: The data sets and flux climatologies (NCAR Technical Note NCAR/TN-460+STR). <https://doi.org/10.5065/D6KK98Q6>
- Marshall, J., Adcroft, A., Hill, C., Perelman, L., & Heisey, C. (1997). A finite-volume, incompressible Navier Stokes model for studies of the ocean on parallel computers. *Journal of Geophysical Research*, *102*, 5753–5766. <https://doi.org/10.1029/96JC02775>
- McGregor, S. (2014). Recent Walker circulation strengthening and Pacific cooling amplified by Atlantic warming. *Nature Climate Change*, *4*, 888–892. <https://doi.org/10.1038/nclimate2330>
- McGregor, S., Sen Gupta, A., & England, M. H. (2012). Constraining wind stress products with sea surface height observations and implications for Pacific Ocean sea level trend attribution. *Journal of Climate*, *25*, 8164–8176. <https://doi.org/10.1175/JCLI-D-12-00105.1>
- McPhaden, M. J., Busalacchi, A. J., Cheney, R., Donguy, J. R., Gage, K. S., Halpern, D., et al. (1998). The Tropical Ocean-Global Atmosphere (TOGA) observing system: A decade of progress. *Journal of Geophysical Research*, *103*, 14,169–14,240. <https://doi.org/10.1029/97JC02906>
- McPhaden, M. J., & Zhang, D. (2002). Slowdown of the meridional overturning circulation in the upper Pacific Ocean. *Nature*, *415*, 603–608. <https://doi.org/10.1038/415603a>
- Medhaug, I., Stolpe, M. B., Fischer, E. M., & Knutti, R. (2017). Reconciling controversies about the ‘global warming hiatus’. *Nature*, *545*, 41–47. <https://doi.org/10.1038/nature22315>
- Meehl, G. A., Hu, A., Arblaster, J. M., Fasullo, J., & Trenberth, K. E. (2013). Externally forced and internally generated decadal climate variability Associated with the interdecadal Pacific Oscillation. *Journal of Climate*, *26*, 7298–7310. <https://doi.org/10.1175/JCLI-D-12-00548.1>
- Merrifield, M. A. (2011). A shift in western tropical Pacific sea level trends during the 1990s. *Journal of Climate*, *24*, 4126–4138. <https://doi.org/10.1175/2011JCLI3932.1>
- Merrifield, M. A., & Maltrud, M. E. (2011). Regional sea level trends due to a Pacific trade wind intensification. *Geophysical Research Letters*, *38*, L21605. <https://doi.org/10.1029/2011GL049576>
- Merrifield, M. A., Thompson, P. R., & Lander, M. (2012). Multidecadal sea level anomalies and trends in the western tropical Pacific. *Geophysical Research Letters*, *39*, L13602. <https://doi.org/10.1029/2012GL052032>
- Meyssignac, B., Salas y Melia, D., Becker, M., Llovel, W., & Cazenave, A. (2012). Tropical Pacific spatial trend patterns in observed sea level: Internal variability and/or anthropogenic signature? *Climate of the Past*, *8*, 787–802. <https://doi.org/10.5194/cp-8-787-2012>
- Moon, J.-H., & Song, Y. T. (2013). Sea level and heat content changes in the western North Pacific. *Journal of Geophysical Research: Oceans*, *118*, 2014–2022. <https://doi.org/10.1002/jgrc.20096>
- Moon, J.-H., Song, Y. T., Bromirski, P. D., & Miller, A. J. (2013). Multidecadal regional sea level shifts in the Pacific over 1958–2008. *Journal of Geophysical Research: Oceans*, *118*, 7024–7035. <https://doi.org/10.1002/2013JC009297>
- Palanisamy, H., Meyssignac, B., Cazenave, A., & Delcroix, T. (2015). Is anthropogenic sea level fingerprint already detectable in the Pacific Ocean? *Environmental Research Letters*, *10*, 84024. <https://doi.org/10.1088/1748-9326/10/8/084024>
- Parker, D. E., Willett, K. M., Allan, R., Schreck, C., & Arndt, D. S. (2016). The 2015/16 El Niño compared with other recent events, *State of the Climate in 2015, Special Supplement to the Bulletin of the American Meteorological Society* (vol. 97, pp. S5–S6).
- Peysner, C. E., & Yin, J. (2017). Interannual and decadal variability in tropical Pacific Sea level. *Water*, *9*, 6. <https://doi.org/10.3390/w9060402>
- Piecuch, C. G. (2017). A note on practical evaluation of budgets in ECCO version 4 release 3 (Tech Rep.) Lexington, MA: Atmospheric and Environmental Research, Inc. Retrieved from <http://hdl.handle.net/1721.1/111094,&urlscore=ftp://ecco.jpl.nasa.gov/Version4/Release3/doc/v4r3&urlscore=budgets&urlscore=howto.pdf>
- Piecuch, C. G., Heimbach, P., Ponte, R. M., & Forget, G. (2015). Sensitivity of contemporary sea level trends in a global ocean state estimate to geothermal fluxes. *Ocean Modelling*, *96*, 214–220. <https://doi.org/10.1016/j.ocemod.2015.10.008>
- Piecuch, C. G., & Ponte, R. M. (2011). Mechanisms of interannual steric sea level variability. *Geophysical Research Letters*, *38*, L15605. <https://doi.org/10.1029/2011GL048440>
- Piecuch, C. G., & Ponte, R. M. (2012). Buoyancy-driven interannual sea level changes in the southeast tropical Pacific. *Geophysical Research Letters*, *39*, L05607. <https://doi.org/10.1029/2012GL051130>
- Piecuch, C. G., & Ponte, R. M. (2013). Buoyancy-driven interannual sea level changes in the tropical south Atlantic. *Journal of Physical Oceanography*, *43*, 533–547. <https://doi.org/10.1175/JPO-D-12-093.1>
- Piecuch, C. G., Ponte, R. M., Little, C. M., Buckley, M. W., & Fukumori, I. (2017). Mechanisms underlying recent decadal changes in subpolar North Atlantic Ocean heat content. *Journal of Geophysical Research: Oceans*, *122*, 7181–7197. <https://doi.org/10.1002/2017JC012845>

- Pillar, H. R., Johnson, H. L., Marshall, D. P., Heimbach, P., & Takao, S. (2018). Impacts of atmospheric reanalysis uncertainty on Atlantic overturning estimates. *Journal of Climate*, *31*, 8719–8744. <https://doi.org/10.1175/JCLI-D-18-0241.1>
- Qiu, B., & Chen, S. (2012). Multidecadal sea level and gyre circulation variability in the northwestern tropical Pacific Ocean. *Journal of Physical Oceanography*, *42*, 193–206. <https://doi.org/10.1175/JPO-D-11-061.1>
- Redi, M. H. (1982). Oceanic isopycnal mixing by coordinate rotation. *Journal of Physical Oceanography*, *12*, 1154–1158. [https://doi.org/10.1175/1520-0485\(1982\)012<1154:OIMBCR>2.0.CO;2](https://doi.org/10.1175/1520-0485(1982)012<1154:OIMBCR>2.0.CO;2)
- Stammer, D., Cazenave, A., Ponte, R. M., & Tamisiea, M. E. (2013). Annual review of marine science, 5, 21–46. <https://doi.org/10.1146/annurev-marine-121211-172406>
- Timmermann, A., McGregor, S., & Jin, F.-F. (2010). Wind effects on past and future regional sea level trends in the southern Indo-Pacific. *Journal of Climate*, *23*, 4429–4437. <https://doi.org/10.1175/2010JCLI3519.1>
- Watanabe, M., Shiogama, H., Tatebe, H., Hayashi, M., Ishii, M., & Kimoto, M. (2014). Contribution of natural decadal variability to global warming acceleration and hiatus. *Nature Climate Change*, *4*, 893–897. <https://doi.org/10.1038/nclimate2355>
- Xie, S.-P., & Kosaka, Y. (2017). What caused the global surface warming hiatus of 1998–2013? *Current Climate Change Reports*, *3*, 128–140. <https://doi.org/10.1007/s40641-017-0063-0>
- Yeager, S., & Danabasoglu, G. (2014). The origins of late-twentieth-century variations in the large-scale north Atlantic circulation. *Journal of Climate*, *27*, 3222–3247. <https://doi.org/10.1175/JCLI-D-13-00125.1>
- Yu, L., & Weller, R. A. (2007). Objectively analyzed air-sea heat fluxes for the global ice-free oceans (1981–2005). *Bulletin of the American Meteorological Society*, *88*(4), 527–540. <https://doi.org/10.1175/BAMS-88-4-527>